Epitaxial Growth of Germanium and Silicon Nanowires by Chemical Vapor Deposition

Christopher J. Hainley

Mechanical Engineering, The University of Portland

NNIN REU Site: Microelectronics Research Center, The University of Texas at Austin
NNIN REU Principal Investigator: Prof. Emanuel Tutuc, Electrical Engineering, The University of Texas at Austin
NNIN REU Mentor: Kamran Varahramyan, Electrical Engineering, The University of Texas at Austin
Contact: chainley@up.edu, etutuc@mer.utexas.edu

Abstract

Germanium (Ge) and silicon (Si) nanowires promise to become useful in the further miniaturization of integrated circuits because they allow for precise structuring at scales of 20-50 nm [1]. In order to accurately characterize the electrical properties of nanowires, a necessary ingredient to any semiconductor device integration route, a reproducible process to fabricate them must be established. Chemical vapor deposition (CVD) presents itself as a useful technique in the fabrication of nanowires by utilizing the vapor-liquid-solid (VLS) mechanism, which also allows for the heterogeneous integration of semiconductor nanowires.

Using 2% diluted SiH_4 and GeH_4 in He as precursor gases in controlled pressure and temperature conditions, and with gold (Au) nanoparticles as catalysts for VLS wire growth, epitaxial growth of Ge and Si nanowires on silicon <111> wafers is demonstrated.

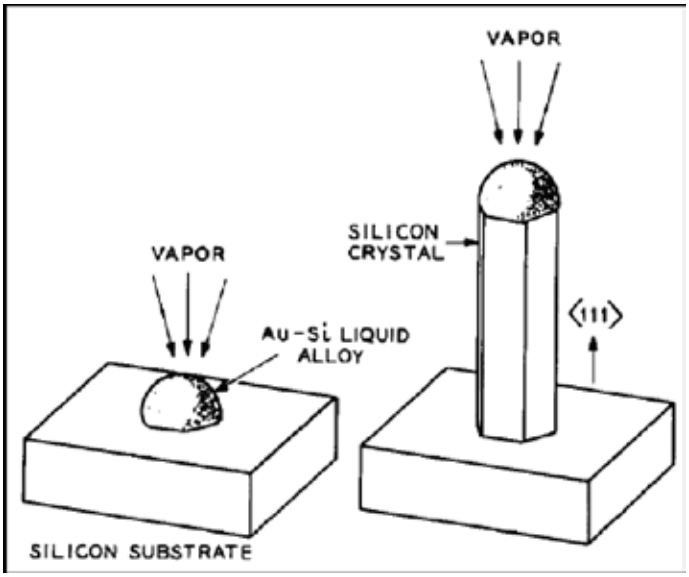

Figure 1: VLS whisker growth [1]. (a) Initial Au droplet absorbs precursor vapor and becomes supersaturated Si-Au alloy. (b) Si from the supersaturated droplet migrates to the crystal lattice of the substrate and forms a silicon whisker in the <111> direction.

Introduction

The VLS growth mechanism of highly anisotropic silicon crystals, or "whiskers," was introduced by Wagner, et al. (Figure 1) [2]. Their study concluded that whisker growth required an impurity and that supersaturated liquid alloy droplets existed on the whisker tips. Subsequent studies have demonstrated reduced whisker sizes down to the nanoscale in silicon [3,4], germanium [5], and III-V compounds [6].

CVD of silicon and germanium nanowires utilizes VLS transport, in which a gold catalyst provides lower dissociation energy (rather than the bare substrate) for the decomposition of the carrier gas, H2, from the precursor, Si or Ge, in the following reactions at the vapor-liquid interface:

$$SiH_4(g) \rightarrow Si + 2H_2(g)$$
$$GeH_4(g) \rightarrow Ge + 2H_2(g)$$

The semiconductor material then diffuses through the droplet, which is liquid at growth temperatures as it forms an eutectic alloy with the Au. Once supersaturated, the semiconductor atoms are incorporated into the crystal lattice at the liquid-solid interface, with epitaxial growth in the <111> direction.

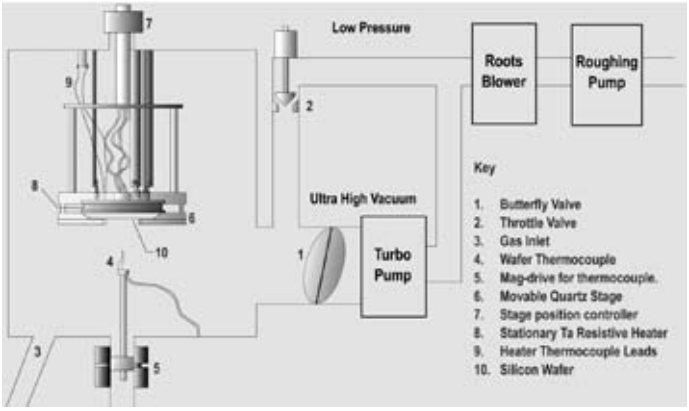

Figure 2: Schematic representation of the CVD apparatus used in the study.

Process

The growth apparatus (Figure 2) used here was a cold wall CVD reactor containing a tantalum (Ta) resistive heater encased in quartz, with operating pressure range of 10^{-8} Torr to 20 Torr. A 1/4 inch gap existed between the wafer and the heater, causing a difference in heat transfer when a precursor gas was or was not present. Thermocouples directly contacting the filaments monitored heater temperatures. Heater voltages and current were also monitored. An unfixed thermocouple measured the wafer temperature.

Silicon <111> wafers were prepared by a 45 second hydrofluoric acid (HF) dip, rinsed, and transferred within 10 minutes to a high vacuum ($\sim 5.0 \times 10^{-6}$ Torr) metal deposition chamber. After depositing a 10Å gold (Au) film, the wafer was transferred into the CVD chamber (approximately 1 hr after HF dip).

Germanium nanowires were produced in a two step process. First, the wafer temperature was raised to 400°-450°C for 5-10 minutes in order for the Au film to coalesce into droplets. The wafer temperature was then lowered within 30 min to a specified temperature, ranging from 230° to 280°C, and GeH_4 was introduced. The reactor pressure was maintained at 10 Torr.

Similarly, silicon nanowires were produced by raising the wafer temperature to 530°-580°C in 60-90 min and introducing SiH_4 into the chamber, maintaining reactor pressure at 10 Torr.

Results

In order to establish Ge wire growth, a series of growths at substrate temperatures of 300°C, 275°C, and 240°C were performed. High temperatures produced tapered wires, a result of the combination of axial and conformal growth. Figure 3 shows the scanning electron microscopy (SEM) data of Ge wire growth carried out at a pressure of 10 Torr and a substrate temperature of ~ 240°C. The measured nanowire growth rate was ~ 1.5 μm/hr, with a nanowire aspect ratio of 33:2.

Si wires were produced at a growth pressure of 10 Torr, with wafer temperatures of 580°C, 550°C, and 530°C. Epitaxial growth was less pronounced than in the Ge growths. Figure 4 shows, at 2 hours, a silicon wire growth maintained at a pressure of 10 Torr and wafer temperature of ~ 580°C. The axial nanowire growth rate was ~ 5 μm/hr, with a nanowire aspect ratio of 40:1. The wires grown at a higher temperature showed a significant surface roughness.

Future Work

The current apparatus separates the heater from the wafer, which results in a wafer temperature dependence on the precursor pressure as well as a large temperature gradient between the heater and wafer. To mitigate these issues, a replacement boron nitride heater will be installed directly contacting the wafer, also allowing for higher wafer temperatures during growth.

Once grown, the nanowires will be deposited onto dielectric wafers, and we will fabricate three terminal, back-gate devices with metal contacts, allowing electronic properties to be characterized.

Acknowledgments

I would like to thank Prof. Tutuc, Kamran Varahramyan, Junghyo Nah, En-shao Liu, and James Ferrara for their help in familiarizing me with the project, Ms. Melanie-Claire Mallison and Ms. Jean Toll for their work in helping me to participate in this program, and National Science Foundation, the National Nanotechnology Infrastructure Network REU Program, and Dr. Banerjee for assisting in funding this research.

References

[1] H.J Fan, P. Werner, M. Zacharias, Small 2006, 701.
[2] R. S. Wagner, W. C. Ellis, Appl.Phys.Lett. 1964, 4, 89.
[3] Y. Wu, R. Fan, P. Yang, Nano Letters 2002, 2, No. 2, 83.
[4] Y. Wu, P. Yang, J.Am. Chem. Soc. 2001, 123, 3165.
[5] H. Dai, D. Wang, Angew. Chem.Int.Ed. 2002, 41, No. 24, 4783.
[6] X. Duan, C.M. Lieber, Adv.Materials, 2000, 12, No. 4, 298.

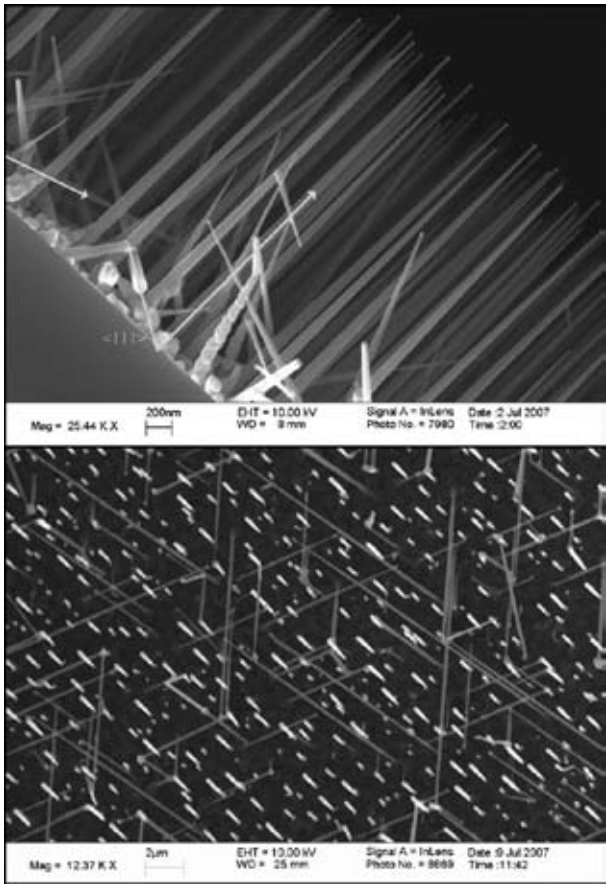

Figure 3, top: Cross-sectional SEM image of showing growth along the three <111> directions, predominately vertical, demonstrating epitaxial Ge nanowire growth on a Si substrate.

Figure 4, bottom: Top down SEM image of silicon nanowires. The three <111> growth directions, aside from the normal to the substrate, can be clearly seen.

Parametric Investigation of Picoliter Droplet Interfacial Tension using a Microfluidic Device

Kevin Kelley

Chemistry and Physics, Pomona College

NNIN REU Site: Center for Nanotechnology, University of Washington
NNIN REU Principal Investigator: Dr. Daniel Chiu, Chemistry, University of Washington
NNIN REU Mentor: Gavin Jeffries, Chemistry, University of Washington
Contact: kevin.kelley@pomona.edu, chiu@chem.washington.edu

Abstract

The transport and detection of nanoscale objects has become an essential part of sub-cellular biochemical research and with it the use of droplets as controllable confined volumes. To fully understand and utilize the chemical environment of droplet systems, it is necessary to elucidate the physical properties of the droplet interface, namely through studying system parameters such as the interfacial tension. The interfacial tension (IFT) is an important physical factor for designing and calculating fluidic dynamics in microfluidic droplet systems. In fluid dynamics, the capillary number (Ca) represents the relative effect of viscous forces versus surface tension acting across an interface between two immiscible liquids. Using Ca, it is possible to simulate fluidic channels and better aid in design, and explain phenomenon.

Introduction

This project seeks to investigate changes in the interfacial tension as a function of the following factors: ion concentration, surfactant type, surfactant concentration, and oil type. The interfacial tension of numerous individual droplets was measured by examining the deformation and restoration dynamics of the drops through a microfluidic channel constriction. Droplet generation parameters were independently varied and results were captured using fast imaging techniques. This video data was analyzed using a mathematical model of droplet dynamics, coded with the program Labview, which calculated the interfacial tensions.

These results will attempt to further clarify the quantitative relationship among the key factors, and should provide general trends for the interfacial tension as system variances are made, allowing future research the ability to predict the effect on droplet formation when used in microfluidic devices for bio-analytical applications.

Design and Fabrication

This microfluidic approach to measure IFT observes the response of individual droplets in a carrier fluid to deformation. A microfluidic tensiometer device should; (a) produce controllably sized droplets, (b) accelerate the droplets, and (c) induce drop deformation and restoration. We designed a system to generate aqueous plugs using a T-junction with an aqueous inlet and an oil inlet. To achieve independent control of the inter droplet distance as well as the droplet velocity, they are accelerated via flow focused oil lines coming from a single inlet.

Droplet deformation occurs in a flow field generated by a microchannel constriction. We experimentally determined that a constriction width of 200 μm induces modest deformations, to which the Taylor theory applies. A thickness of about 200 μm throughout was determined to be optimal.

Silicon masters patterned with SU-8 photoresist were fabricated using photolithography as described in detail elsewhere. Briefly, in order to create channels of 200 μm thickness, it was necessary to successively spin two 100 μm layers of SU-8. These were exposed to UV through a patterned mask, and then developed using propyl glycol methyl ether acetate (PGMEA).

To form the microchannels, the pattern on the master was replicated in poly(dimethylsiloxane) (PDMS) and then sealed with oxygen plasma to a coverslip with a thin layer of spin-coated PDMS. It was necessary to coat the coverslip with PDMS because the generation of aqueous droplets required channels with four hydrophobic walls to prevent wetting by the aqueous phase of the walls of the channel.

To address the microchannels, access holes to the channels were punched with a 16-gauge needle. Polyethylene tubing (PE 100) was inserted into the access holes and then attached to a microinjector, with the aqueous and two oil inlets having their own respective injector.

Parameters Tested

The continuous phase type and its viscosity have significance on the experiment. High viscous oils generally make very stable small droplets easier than low viscosity oils. The compatibility of the oil with the sample is also important since biological samples require low mass transfer between the oil and water and vice versa to maintain droplet constant concentrations.

Surfactants are known to reduce the interfacial tension at the oil-water interface and are necessary to create stable droplets in most systems. Similarly, different types of surfactants have varying compatibilities with both the continuous and dispersed phases.

When using biological samples, the pH of the system becomes important. The ion concentration is dependent on the pH. An investigation of the affects of ion concentration on the affects of interfacial tension is thus important.

Results and Conclusions

Interfacial tension was calculated by using a custom built Labview program that would track the vertical deformation of the droplets as a function of position. By measuring the time for drop shape relaxation, the interfacial tension could be calculated.

The results demonstrate that interfacial tension correlates positively with oil viscosity, negatively with surfactant concentration, and negatively with ion concentration (Figures 1-3). The three surfactant types tested (Gran Surf 77, Tween 20, and Span 85) were found to have no correlation with the interfacial tension (not shown). It is well known that surfactant concentration correlates negatively with interfacial tension. The fact that ion concentration correlates negatively with interfacial tension was a surprising result. Intuitively, we would expect that an increase in ions would cause the water phase to be more dissimilar to the oil phase, which would cause an increase in interfacial tension.

In conclusion, we successfully developed a microfluidic device that rapidly measured interfacial tension of picoliter droplets, and have shown that surface active components indeed affect the interfacial tension. These results can be used to extrapolate interfacial tension values so as to extrapolate the optimal microfluidic chip design

Acknowledgements

I would like to thank NSF and the National Nanotechnology Infrastructure Network REU Program for making this all possible. Special thanks to my PI, Dr. Daniel Chiu, and especially my mentor, Gavin Jeffries, for all his time and help.

References

[1] Cabral, J.T., and Hudson, S.D.; "Microfluidic approach for rapid multicomponent interfacial tensiometry"; Lab on a Chip, 6, 427-436 (2006).

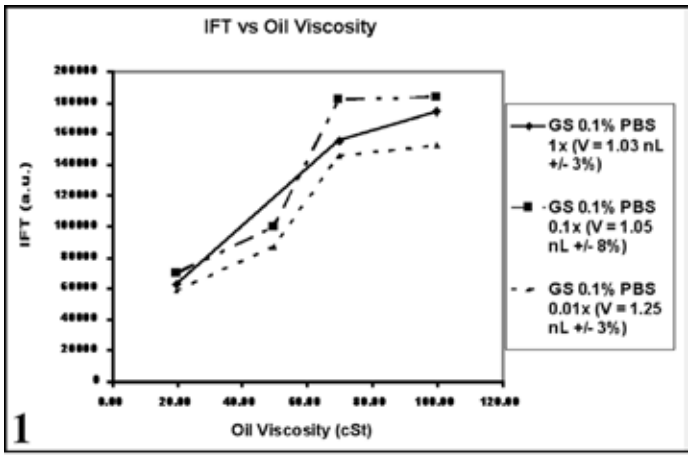

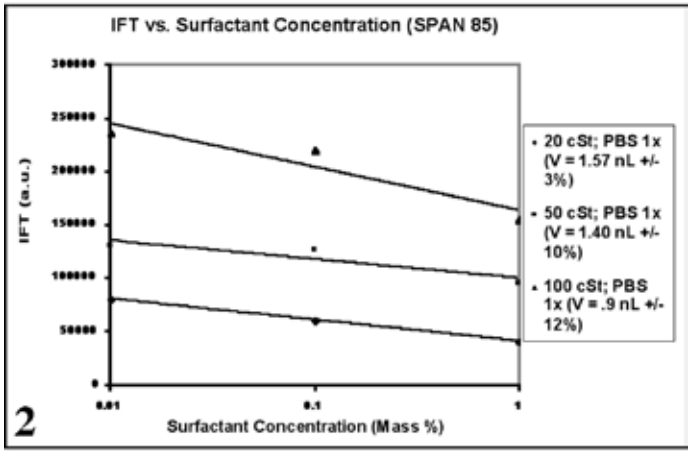

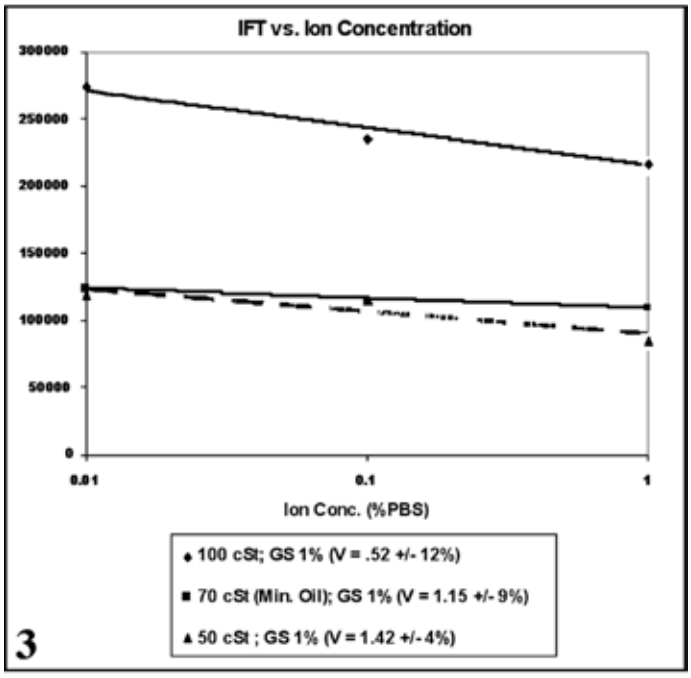

Figure 1: IFT as a function of oil viscosity at three different ion concentrations.

Figure 2: IFT as a function of surfactant concentration for three different oils.

Figure 3: IFT as a function of ion concentration for three different oils.

Rapid Synthesis of Silver Nanowires

Kylee Korte

Chemistry, Bradley University

NNIN REU Site: Center for Nanotechnology, University of Washington
NNIN REU Principal Investigator:Professor Younan Xia, Chemistry, University of Washington
NNIN REU Mentor: Dr. Sara Skrabalak, Chemistry, University of Washington
Contact: kkorte@mail.bradley.edu, xia@biomed.wustl.edu, skrabs@u.washington.edu

Abstract

The presence of either copper(I) or copper(II) chloride in the polyol reduction of silver nitrate facilitates the production of silver nanowires. Silver nanowires have applications in many areas, including electronics and catalysis. These wires are produced quickly (in approximately one hour), with the synthesis being easily performed in disposable glass vials, using only pipettes to deliver reagents. Specifically, silver nitrate is reduced by ethylene glycol in the presence of poly(vinylpyrrolidone) (PVP) and copper(II) chloride. PVP acts as a stabilizing agent, while the copper chloride likely controls the rate of silver(I) reduction and initial seed formation. Our results indicate that both the copper and chloride ions are necessary to synthesize the wires; otherwise, ill-defined silver particles are formed. Scanning electron microscopy (SEM) has been used to characterize the wires.

Introduction

Metallic nanostructures have a wide range of properties and applications. These properties and applications are determined by the shape, size, structure, and composition of the nanostructures. The presence of various ions has been shown to influence the shape and size of metallic nanostructures produced via the polyol method. For example, previous research done by the Xia group has shown that the presence of iron(II) or iron(III) ions in the polyol synthesis facilitates the growth of silver nanowires or cubes, depending on the concentration of the iron ions [1]. A study of copper salts has shown that the presence of copper(I) or copper(II) chloride in the polyol reduction of silver nitrate allows for the production of silver nanowires, which can be used in many areas, including electronics and catalysis [2].

Experimental Procedure

The polyol method involves the reduction of a metal salt precursor by a polyol, a compound containing multiple hydroxyl groups. The polyol used in this synthesis, ethylene glycol, served as both the reducing agent and solvent. 5 mL of ethylene glycol was heated at 150°C for one hour with stirring (260 rpm). This pre-heating was done in disposable glass vials placed in an oil bath. 40 μL of a 4 mM $CuCl_2 \cdot 2H_2O$/ethylene glycol solution was added, and the solution was allowed to heat for 15 minutes. 1.5 mL 114 mM PVP/ethylene glycol was then added to each vial, followed by 1.5 mL 94 mM $AgNO_3$/ethylene glycol. All reagents were delivered by pipette. The reaction was stopped when the solution became gray and wispy, after approximately one hour. The reaction was stopped by submerging the vials in cold water. The product was washed once with acetone and three times with deionized water.

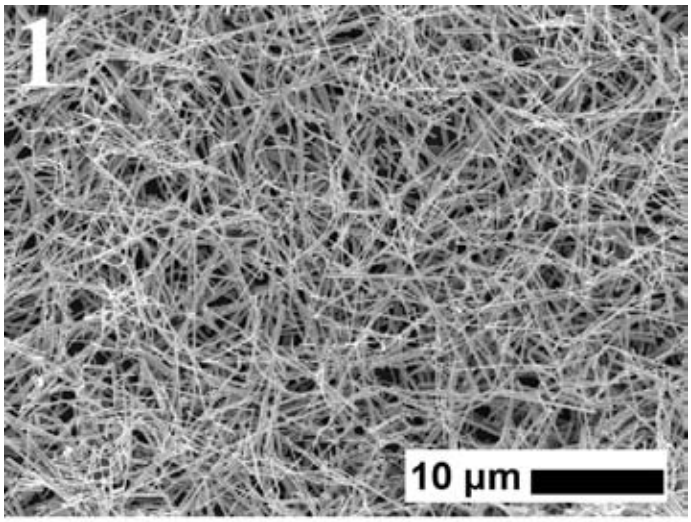

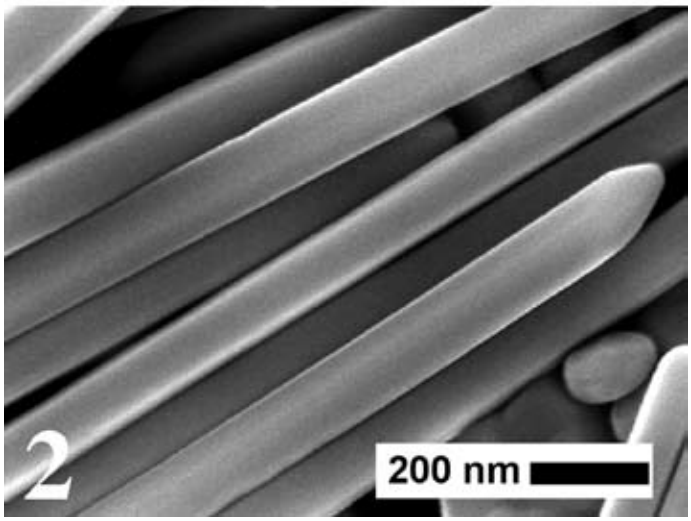

Figure 1: SEM of silver nanowire.

Figure 2: Higher magnification SEM of silver nanowires.

Results and Conclusions:

The produced wires were relatively uniform in shape and size. They had a pentagonal cross-section, as determined by scanning electron microscope (SEM), and were, on average, approximately 10-50 μm in length.

These wires were also present in high yield (approximately 90% relative to other structures) and were produced in approximately one hour after the addition of all reagents. Figures 1 and 2 show SEM images of the wires produced.

One of the advantages of this particular synthesis is its simplicity. To avoid supersaturation of the reaction media and thus particle formation, typically a syringe pump is required to controllably add reagents. Here, we are able to prepare silver wires in high yield without a syringe pump, which may not be available in all laboratories due to costs. The vial setup allows the reaction to be scaled up by simply running the reaction in additional vials. This setup of vials also allows a range of variables, such as concentration or temperature, to be tested at once.

To elucidate the role of copper(II) chloride, several controls were run. Sodium chloride and copper(II) nitrate were used to test the effect of each ion on this synthesis (sodium and nitrate ions are spectators and should have no effect on this synthesis). As shown in Figure 3, when only copper(II) nitrate is present, only particles are produced. Similarly, as shown in Figure 4, when only sodium chloride is present, only particles are produced. However, when both copper(II) nitrate and sodium chloride were added, wires were produced, indicating that both ions are necessary for wire growth.

Previous reports indicate that chloride ions can help stabilize initial silver seeds, preventing agglomeration, while Cl^-/O_2 has been shown to etch seeds [3]. To further investigate the function of copper(II) in this synthesis, further experiments were performed using copper(I) chloride. As with copper(II) chloride, copper(I) chloride facilitates silver wire formation. This result suggests that the redox behavior of the copper additives helps to control the reduction of silver nitrate and avoid initial supersaturation.

Future Work

To better understand this proposed mechanism, trials run in an inert atmosphere are now underway to determine the role of oxygen in this synthesis.

Acknowledgments

Special thanks to my mentor, Sara Skrabalak, for her guidance and support. I would also like to thank Professor Younan Xia, the other members of the Xia group, and Dr. Ethan Allen. This research was supported by the 2007 National Nanotechnology Infrastructure Network Research Experience for Undergraduates and the National Science Foundation. Thank you to all for a memorable summer!

References

[1] Wiley, B., et al; "Polyol Synthesis of Silver Nanostructures: Control of Product Morphology with Fe(II) or Fe(III) Species"; Langmuir, 21, 8077-8080 (2005).

[2] Xia, Y., et al; "One-Dimensional Nanostructures: Synthesis, Characterization, and Applications"; Advanced Materials, 15, 353-389 (2003).

[3] Wiley, B., et al; "Polyol Synthesis of Silver Nanoparticles: Use of Chloride and Oxygen to Promote the Formation of Single-crystal, Truncated Cubes and Tetrahedrons"; Nano Letters, 4, 1733-1739 (2004).

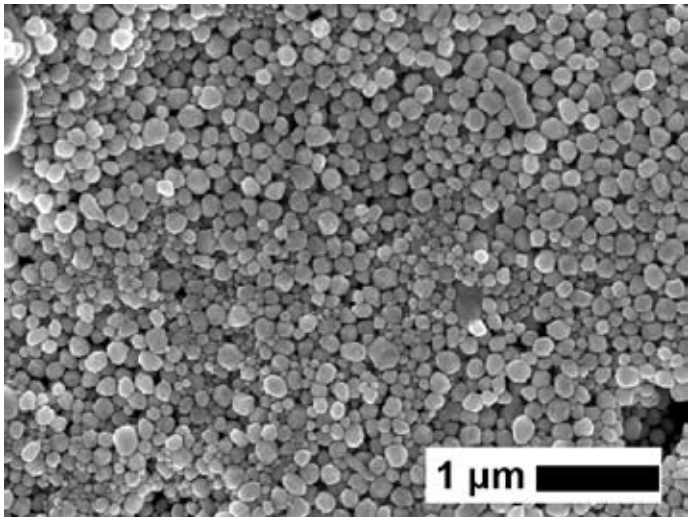

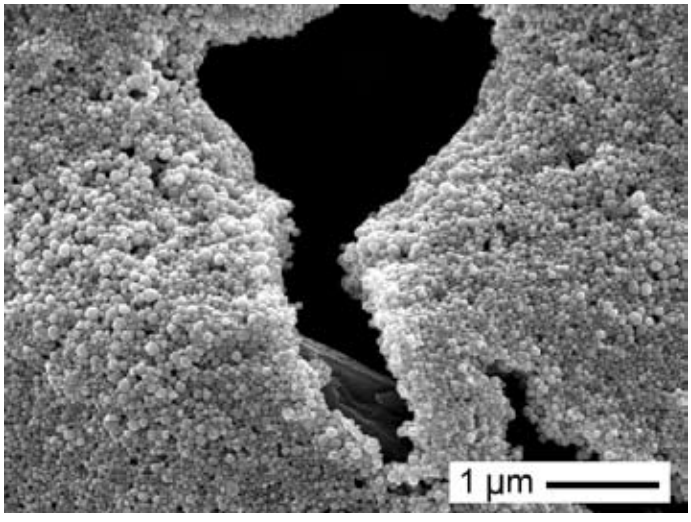

Figure 3, top right: SEM of sample produced in the presence of copper(II) nitrate (no Cl present).

Figure 4, bottom right: SEM of sample produced in the presence of sodium chloride (no Cu present).

Directed Self-Assembly for Post-32 nm Lithography

Brian Lambson

Electrical Engineering, Columbia University

NNIN REU Site: Microelectronics Research Center, Georgia Institute of Technology
NNIN REU Principal Investigator: Raghunath Murali, Microelectronics Research Center, Georgia Institute of Technology
NNIN REU Mentor: Gerald Lopez, Electrical Engineering, Georgia Institute of Technology
Contact: bjl2109@columbia.edu, rm206@mail.gatech.edu

Abstract

Like many large polyaromatic hydrocarbons (PAHs), C96 self-assembles into well-ordered supramolecular structures due to π-π interactions between adjacent molecules. Because densely packed monolayers of C96 fibers are easily obtained on silicon or silicon oxide (SiO_2) via standard deposition techniques such as spin-coating or drop-coating, C96 is an attractive candidate for microelectronics applications. This project explores the possibility of using directed self-assembly to attain long-range ordering of C96 fibers for use in post-32 nm lithography. In this method, top-down lithography defines the pattern placement, and C96 self-assembly defines the pattern line-width. Experimental results demonstrate consistently strong C96 fiber alignment with 250 nm and 125 nm chromium (Cr) trenches, suggesting that with further process optimization, directed C96 self-assembly may be a viable extension of traditional lithography techniques.

Introduction

In lithography, the term "critical dimension" refers to the smallest feature size that can be accurately reproduced using a given technology. If current rates of progress in electronic device scaling are maintained, sub-16 nm dimensions will be reached within the next decade [1]. Optical lithography, currently the standard lithography technique for large-scale semiconductor fabrication, has achieved critical dimensions at the 32 nm node, but rising costs and fundamental limits may restrict its use at future nodes.

We seek to extend traditional lithography for post-32 nm critical dimensions using a technique called directed C96 self-assembly. C96 is a large polyaromatic hydrocarbon (PAH) that self-assembles on silicon or SiO_2 into long fibers 2-3 nm in diameter, as shown in Figure 1. Looking down over the substrate, C96 self-assembly results in a dense two-dimensional fiber network that can serve as an etch mask to transfer the pattern onto the substrate [2]. In this case, the critical dimension of C96 self-assembly is the fiber width. The primary drawback of existing C96 self-assembly methods is that C96 fibers tend to orient randomly, rendering the resulting patterns unusable for many practical applications.

Our objective is to develop a method to control the orientation of C96 fibers. One candidate is directed self-assembly, in which patterned features created by traditional lithography techniques direct the self-assembly of C96 fibers. Top-down lithography defines the pattern placement, and C96 self-assembly defines the pattern line-width. In our experiment, we qualitatively examine the interaction of C96 fibers with patterned metal trenches and determine the degree to which C96 fiber orientation is correlated to trench direction.

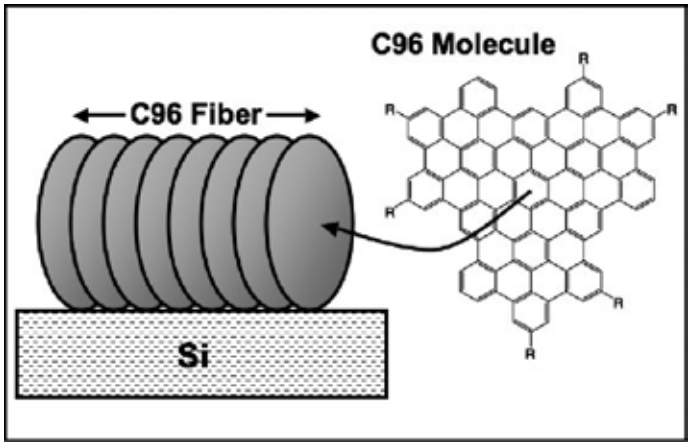

Figure 1: C96 self-assembly mechanism.

Experimental Procedure

A silicon wafer was first patterned via electron-beam lithography (EBL), followed by a metal liftoff. Line/space patterns—parallel lines of fixed width—were patterned onto ZEP 520A resist using a JEOL JBX-9300FS EBL system, with line-widths ranging from 125 nm to 1 μm. After developing the resist, we evaporated 8 nm Cr on the sample and performed a liftoff process using n-methyl-pyrrolidone. The end result was a pattern of parallel Cr trenches, 8 nm deep and 125 nm to 1 μm wide.

C96 deposition was accomplished using one of two methods, dropcast or spincast. In both methods, we first dissolved crystalline C96 in chloroform ($CHCl_3$) at a concentration of 10^{-5} M. Dropcasting involves applying several drops of the C96 solution directly onto a patterned sample and allowing the solvent to evaporate overnight. Spincasting differs from dropcasting in that we spun the sample at 1000 rpm for 60 seconds immediately after depositing the C96 solution, eliminating the need for overnight evaporation.

Before imaging the sample, all C96 molecules that had not bonded covalently to the silicon substrate were removed with chloroform via Soxhlet extraction. Once clean, the sample was imaged using an atomic force microscope (AFM), which allowed us to determine the location and orientation of the C96 fibers. Though the AFM has excellent vertical resolution, lateral resolution is dependent on the width of the probe tip, approximately 25 nm. Therefore, imaged fibers appeared about ten times their actual width of 2-3 nm, limiting our ability to quantitatively analyze the surface patterns.

Results

Samples were prepared using the experimental procedure for Cr line-widths of 1 μm, 250 nm, and 125 nm. Our conclusions are based on qualitative observations regarding the correlation between the C96 fiber orientation and the trench walls, as seen in AFM images.

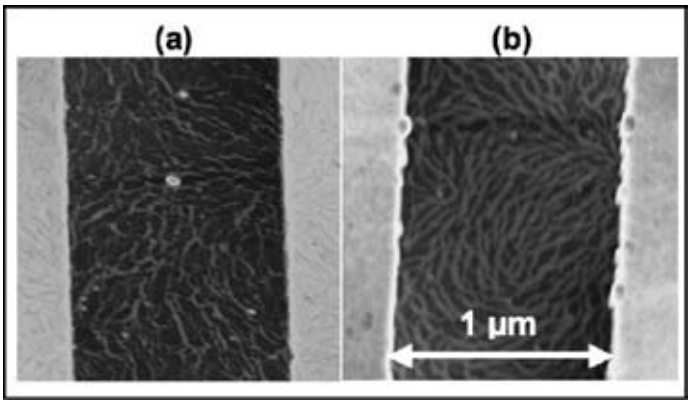

Figure 2: 1 µm trenches, (a) spincoated and (b) dropcoated.

We first noted that dropcast deposition is preferable to spincast deposition. The spincast samples, such as the sample shown in Figure 2a, demonstrated incomplete C96 fiber formation and limited correlation with the trench direction. In Figure 2b, a dropcast sample with the same 1 μm Cr line-width yielded much more robust fiber formation, but equally lacked correlation with the trench direction.

For 250 nm and 125 nm Cr line-widths, however, dropcast samples demonstrated excellent C96 fiber alignment, as shown in Figures 3 and 4. Additionally, on the 125 nm samples, we observed consistency perpendicular to the trench direction—there were approximately two C96 fibers in parallel in each trench. These results confirm the ability to influence C96 fiber alignment using a directed self-assembly method.

Conclusions

We developed and tested a procedure that allows for long-range control of C96 fiber alignment using a directed self-assembly method. First, we showed that C96 fibers tend to self-align with 250 nm-wide patterned Cr trenches. Later, in 125 nm trenches, we observed a significant degree of control over the number of fibers that align in parallel in each trench.

We conclude that, with optimization, directed C96 self-assembly has the potential to be used in large-scale semiconductor fabrication as a practical lithography technique offering sub-32 nm critical dimensions.

Acknowledgements

I would like to thank Gerald Lopez, Dr. Raghunath Murali, Dr. James Meindl, Dr. Jonas Jarvholm, Jennifer Root, and the Tolbert Group for their assistance. This project was funded by Georgia Tech, the National Nanotechnology Infrastructure Network Research Experience for Undergraduates Program, and the National Science Foundation.

References

[1] "Lithography," in International Technology Roadmap for Semiconductors, 2005.

[2] J. Jarvholm, "Etch resistance for highly aromatic monomolecular etch masks," Atlanta: Georgia Tech, 2007.

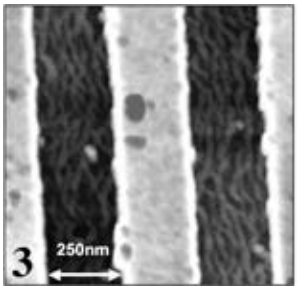

Figure 3, left: 250 nm trenches, dropcoated.

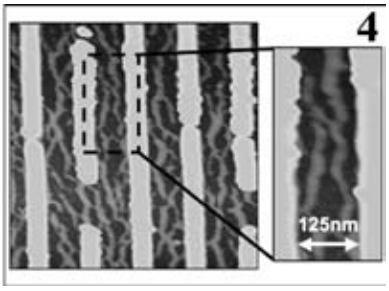

Figure 4, right: 125 nm trenches, dropcoated.

Factors that Affect the Synthesis of Gold Nanorods

Alice MacQueen

Biology and Biochemistry, University of Virginia

NNIN REU Site: Microelectronics Research Center, The University of Texas at Austin
NNIN REU Principal Investigator: Brian A. Korgel, Chemical Engineering, The University of Texas at Austin
NNIN REU Mentor: Danielle K. Smith, Chemical Engineering, The University of Texas at Austin
Contact: alicem@virginia.edu, korgel@che.utexas.edu, dsmith@che.utexas.edu

Introduction

Gold nanorods have two plasmon resonance peaks in their absorbance spectra: a higher-energy peak related to their diameter and a lower-energy peak associated with their length. Typically, the low energy peak occurs at ~ 750 nm. Nanorods with an optical signal within the 700-1000 nm range are interesting for medical imaging of tissue at cellular resolutions. This range corresponds to an "optical window" where light absorption is minimal, thus allowing deeper tissue penetration. For example, we have previously explored the use of near-infrared two-photon luminescence (TPL) for epithelial pre-cancer cell detection [1]. Lengthening the nanorods shifts the lower-energy plasmon to longer wavelengths, improving the optical penetration depth.

In this project, we focused on synthesizing gold (Au) nanorods with longitudinal plasmon peaks around 900 nm. We prepared colloidal Au nanorods using a seed-mediated approach and studied the effect of the additives hydrochloric acid (HCl) and sodium sulfide (Na_2S) [2]. Then, we measured absorbance spectra of the Au nanorods, and quantified the nanorod aspect ratios using transmission electron microscopy. Longitudinal plasmon resonances were red-shifted to wavelengths as long as 994 nm by adding both Na_2S and HCl.

Experimental Procedure

Gold nanorods were synthesized in aqueous solutions using a seed-mediated approach. Au seeds were first prepared by adding sodium borohydride (0.01 M, 600 μL) to a preparation of cetyltrimethylammonium bromide (CTAB, 0.1 M, 9.75 mL) and hydrogen tetrachloroaurate (0.01 M, 250 μL), and stirring for two minutes. Next, 12 μL of this gold seed solution was injected into a growth solution containing CTAB (0.1 M, 9.5 mL), silver nitrate (0.01 M, 75 μL), Au tetrachloroaurate (0.01 M, 500 μL), and ascorbic acid (0.1 M, 55 μL). Additional compounds were combined with this "typical" growth solution to adjust the wavelength of the longitudinal plasmon peak.

In the first experiment, hydrochloric acid (0.1 M, varying amounts between 50 and 2000 μL) was added just before injecting the seed solution. The second experiment involved adding sodium sulfide (Na_2S, 0.1 M), which quenches the growth solution [2]. Na_2S was added in two molar ratios of sulfur (S) to metal (M, both Au and Ag) at different times following seed injection (both 15 and 30 minutes afterwards, in a 2:1 and 4:1 S:M ratio). In the third experiment, both hydrochloric acid (0.1 M, amounts between 50 and 1000 μL) and Na_2S (0.1 M, 4:1 S:M ratio at 30 minutes) were added to the growth solution.

The Au nanorods were purified by two cycles of centrifugation at 8500 rpm for 10 minutes, followed by suspension in deionized water. Nanorods were characterized using UV-Vis spectroscopy and transmission electron microscopy.

Results

Experiment 1. Adding up to 500 μL of HCl shifted the lower-energy plasmon resonance peak out to a maximum of ~ 800 nm.

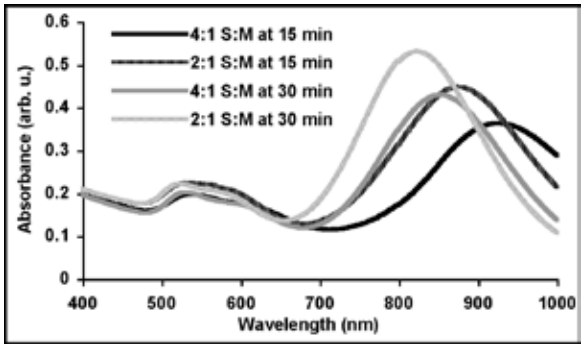

Figure 1: Addition of sodium sulfide to the growth solution.

Larger HCl additions seemed to poison the growth solution, blue-shifting the low-energy peak back toward the wavelength of the control (Figures 1 and 4B). Adding more HCl also lowered the yield of rods, as evidenced by the decreased absorbance ratio between the low- and high-energy peaks. A higher transverse peak, relative to the longitudinal plasmon peak, precluded formation of a higher population of spheres (gold particles without a longitudinal dimension).

Experiment 2. Injecting Na_2S at a larger S:M ratio and shorter time into growth shifted the longitudinal plasmon farther to the red (Figure 2). Changing the time of addition had a greater effect on nanorod length than varying S:M. Also, nanorod yield decreased while red-shifting the longitudinal plasmon.

Experiment 3. Adding Na_2S and up to 100 μL of HCl red-shifted the maximum wavelength of the second plasmon peak to 994 nm. Additional HCl lowered the rod yield and blue-shifted the longitudinal peak away from the 994 nm maximum. As shown in

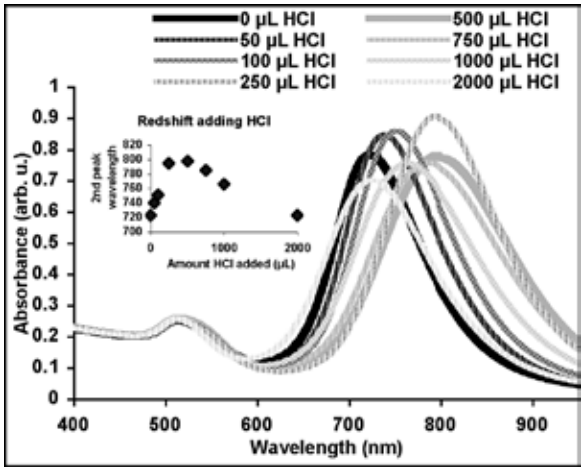

Figure 2: Addition of hydrochloric acid to the growth solution.

Figure 3, adding both Na_2S and HCl during rod growth lowered the longitudinal peak height; thus, rod yield was compromised by including these additives. However, Figure 4C exhibits nanorod samples with an absorbance peak positioned near the lower energy boundary of the "optical window" for cellular imaging, making them interesting agents for TPL imaging.

Conclusions

Longitudinal plasmon resonances were red-shifted as far as 994 nm with the addition of 100 μL 0.1M HCl followed by Na_2S in a 4:1 S:M ratio 30 minutes after the growth reaction was seeded. Adding Na_2S alone could not mimic this result; rods obtained with only Na_2S had a longitudinal peak red-shifted to 925 nm, and were obtained in much poorer yield. Adding HCl alone resulted in nanorods with a longitudinal peak having a maximum red-shift of 800 nm. Larger HCl additions blue-shifted this peak wavelength away from this maximum. Rods with the most potential for TPL imaging were obtained by adding 50 μL 0.1M HCl and. Na_2S at a 4:1 S:M ratio at 30 min, and had a longitudinal peak at 915 nm.

Future Work

Future work could involve increasing the monodispersity of the gold nanorod lengths in these altered procedures, as indicated by the breadth of the longitudinal plasmon peak. The yield of rods could also be increased by more delicately tuning the ratio of sodium sulfide or the time at which it is added.

Acknowledgements

Many thanks to Danielle Smith, Michael Rasch, and Dr. Brian Korgel for their guidance, Jean Toll for her help and organization, and to the National Nanotechnology Infrastructure Network Research Experience for Undergraduates Program, National Science Foundation, and Dr. Sanjay Banerjee for funding this work.

References

[1] Durr, N; Larson, T; Smith, D; Korgel, B; Sokolov, K; Ben-Yakar, A; "2-Photon Luminescence Imaging of Cancer Cells Using Molecularly Targeted Gold Nanorods"; Nanolets. V0 A-E (2007).

[2] Zweifel, D.; Wei, A.; "Sulfide-Arrested Growth of Gold Nanorods"; Chem. Mater., 4256-4261 (2005).

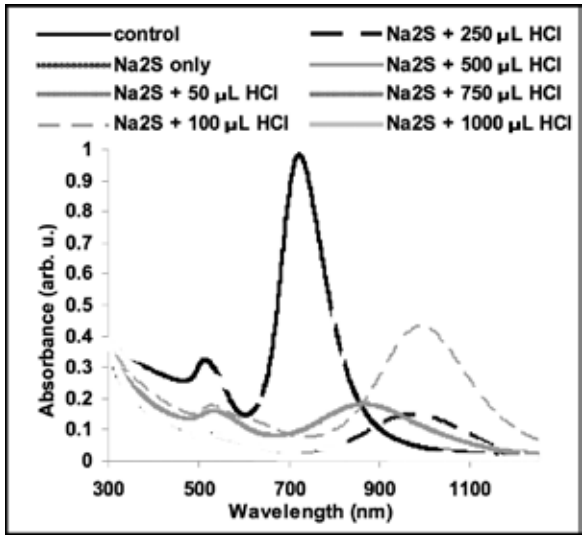

Figure 3: Addition of both HCl and Na_2S to the growth solution.

Figure 4, right: TEMs of gold nanorods synthesized in the presence of various additives with the most red-shifted second plasmon peak.

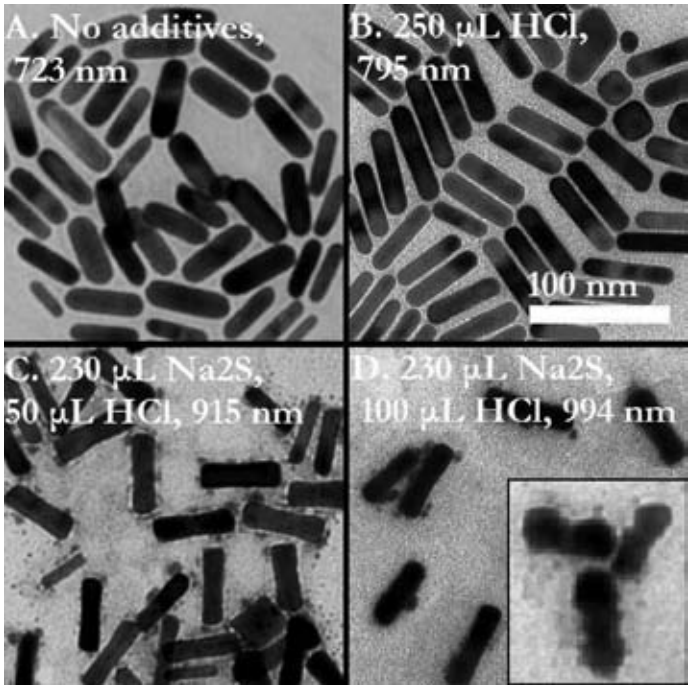

Cadmium Selenium Quantum Dot Photodiodes

Van Nguyen

Chemical Engineering, University of California, Riverside

NNIN REU Site: Center for Nanotechnology, University of Washington
NNIN REU Principal Investigator: Dr. Daniel Gamelin, Chemistry Department, University of Washington, Seattle
NNIN REU Mentor: Paul Archer, Chemistry Department, University of Washington, Seattle
Contact: van.nguyen002@email.ucr.edu, gamelin@chem.washington.edu, archerp@u.washington.edu

Abstract

A simple cadmium selenium (CdSe) quantum dot photodiode was assembled. The device is composed of two electrodes, indium tin oxide (ITO) and ITO/titanium dioxide (TiO_2) plates, two layers of 3-mercaptopropionic acid, and a thin layer of CdSe quantum dots. With this simple configuration, photocurrents up to 0.5 μA were detected under room light excitation. In addition, the diode photocurrent action spectra closely resembled the absorption spectrum of the parent colloidal CdSe quantum dots, indicating CdSe-TiO_2 coupling. Most interestingly, cyclic voltammetry scans revealed the photodiode properties of the device.

Introduction

The emission and absorption spectra of CdSe quantum dots are highly tunable making this one of the most studied nanocrystalline semiconductors. TiO_2 is widely used as an anode material in photovoltaic cells due to its superb performance as a charge carrier. Therefore, a CdSe/TiO_2 coupled system is expected to be an efficient and tunable photoanode.

In the past, CdSe and CdSe/TiO_2 systems have been grown from their precursors on a substrate [1,2]. Such methods yield a densely packed, well-connected nanocrystalline structure, in which the CdSe absorbs visible photons, while the TiO_2 network acts as a charge transfer system. In previous reports, however, the size and shape of the CdSe quantum dots could not be precisely controlled. In contrast, direct deposition of as-prepared quantum dots on TiO_2 coated substrates fails due to poor CdSe-TiO_2 coupling.

Here, we demonstrate an alternative method to assembling an effective photoanode using colloidal CdSe quantum dots and an intermolecular linker, 3-mercaptopropionic acid. The acid linker is a bifunctional molecule in which the thiol group on the linker binds to the CdSe quantum dots, while the carboxylic acid group attaches to the TiO_2 network.

Experimental Procedure

Chemical Preparation. Colloidal CdSe quantum dots were synthesized using the hot injection method as described in Qu, et al., 2001 [3]. By washing extensively with butanol and toluene, excess ligand in solution and on the surface of the CdSe quantum dots were removed. The bare nanocrystals were then suspended in tetrahydrofuran (THF) (Solution 1). In addition, 3-mercaptopropionic acid was diluted in ethanol (Solution 2). Lastly, 0.66 mmol of TiO_2 nanoparticles and 5 drops of polystyrene spheres were suspended in 10 ml of ethanol (Solution 3).

Electrode Preparation. Indium tin oxide (ITO) was chosen due to its transparency and low cost. ITO plates were cut into rectangular pieces, approximately 0.5 × 1.0 in. in dimension. After cleaning with ethanol and toluene, half of the cut ITO plates were spin-coated with Solution 3. These plates were then annealed at 450°C for 30 minutes. Before being stored under dry condition, the plates were rinsed thoroughly with ethanol.

Device Assembly. Solution 2 was drop-coated onto the TiO_2 coated ITO plate. When most of the ethanol had evaporated, Solution 1 was deposited. It took a few hours for the THF to evaporate. After that, an uncoated ITO plate was offset on top, and the whole device was secured using binder clips. Finally, copper tapes were pasted on the edges of the electrodes to enhance electrical connections. The cross sectional view of the device is shown in Figure 1.

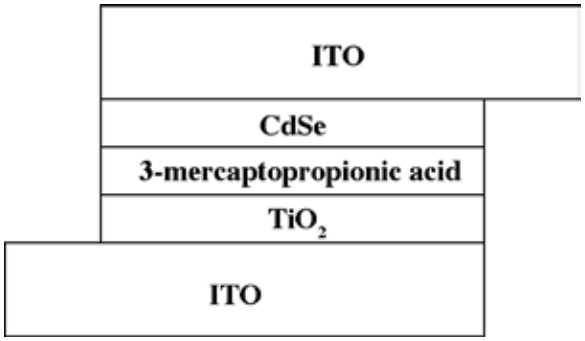

Figure 1: Device configuration (drawing not to scale).

Characterization. All measurements were done using MicroAutoLab-TypeII apparatus.

Result and Conclusions

In Figure 2, the incident photo-to-current conversion efficiency, IPCE4, spectra resembled the absorption spectrum of CdSe colloidal quantum dots at wavelengths longer than 520 nm. In

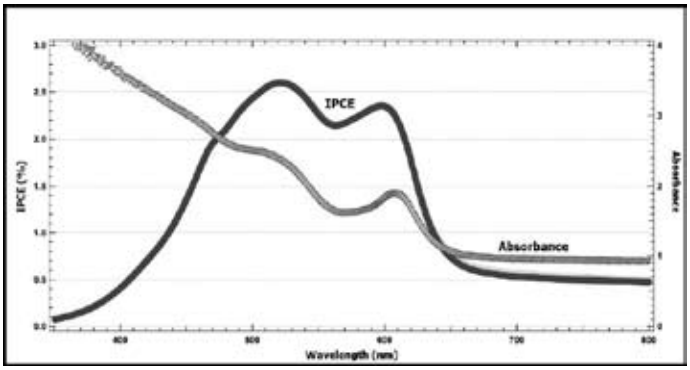

Figure 2: Photocurrent action and absorbance spectra (monochromator rate at 1.44 nm/s; applied potential at1.0 V).

other words, CdSe quantum dots were producing current under photo-excitation.

The most cyclic voltammetry characteristics of the device are presented in Figure 3. The observed current at 1.0 V is 13 times greater than that at -1.0 V. In addition, the cell shows ohmic behavior from 0.0 V-1.0 V. This cyclic voltammetry scan provides strong evidence that the cell possesses photodiode characteristics.

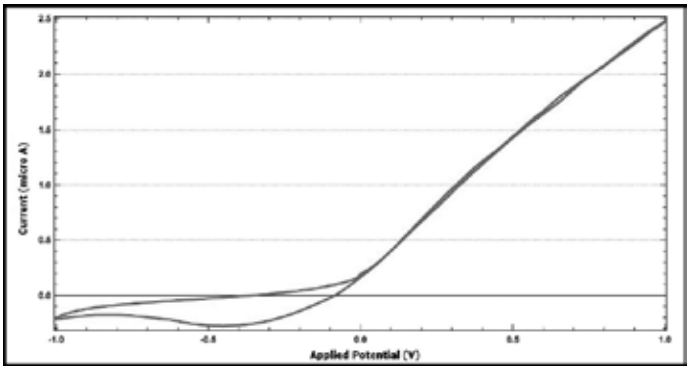

Figure 3: Cyclic voltammetry scans (scan rate at 0.001 V/s; 25 cm below a 20 halogen lamp).

The proposed photoelectrical mechanism of the CdSe-TiO_2 coupled system involves electron tunneling. Upon irradiation, CdSe quantum dots absorb energy and promote electrons from the valence band to the conduction band (exciton generation). The applied voltage then helps inject the excited electrons into the TiO_2 network, and subsequently into the ITO and the closed circuit. Since the valence band offsets between CdSe and either TiO_2 or ITO are large, the holes are confined to the CdSe. In contrast, the conduction band offsets between CdSe and TiO_2 and ITO are relatively small. With sufficient applied potential, electrons could "hop" from the plain ITO plate to re-fill electron deficiencies (see Figure 4).

The probability of successful electron tunneling decreases exponentially with distance. Thus, the ideal position of the holes is in the middle of the film. If the film were too thick, electron tunneling would be greatly inhibited. If the film were too thin, there would not be enough CdSe quantum dots to absorb the photons.

The film used in this project was fairly thick (~ 50 μm). Since the absorption spectrum of the CdSe-TiO_2 system increased dramatically at shorter wavelength (< 500 nm), most photons were absorbed well before they reached the middle region. As a result, charge separation was less efficient and less photocurrent was detected. The decrease in IPCE at wavelengths shorter than 520 nm in Figure 2 is therefore due to the large film thickness.

In conclusion, CdSe-TiO_2 coupled photoelectrodes were successfully prepared using 3-mercaptopropionic acid as a linker. A simple device assembled from these photoelectrodes showed high sensitivity to various wavelengths and possessed photodiode properties.

Acknowledgements

We thank Ethan Allen for laboratory coordination and all members in the Gamelin group at UW for friendly and professional collaboration. Funding for this project was provided by the National Nanotechnology Infrastructure Network Research Experience for Undergraduates Program and National Science Foundation.

References

[1] Diguna, L. J.; Shen, Q.; Kobayashi, J.; Toyoda, T. Applied Physics Letters, 2007, Vol. 91.

[2] Robel, I.; Kuno, M.; Kamat, P. V. J. Am. Chem. Soc. 2007, 129, 4136-4137.

[3] Qu, L.; Peng, A. Z.; Peng, X. Nano Letters, 2001, Vol.1, No. 6, 333-337.

[4] Liu, W; Salley, G.; Gamelin, D. J. Phys. Chem. B 2005, 109.

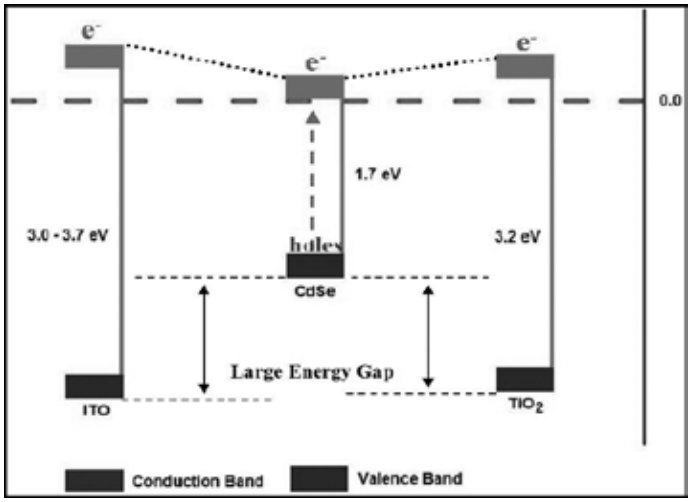

Figure 4: Electron tunneling.

Effect of Hydroxide Surface Treatments on Photoluminescence of InP/InGaAs Heterostructures

Christina Yeung

Engineering, Swarthmore College

NNIN REU Site: Minnesota Nanotechnology Cluster, University of Minnesota-Twin Cities
NNIN REU Principal Investigator: Joey Talghader, Electrical and Computer Engineering, University of Minnesota-Twin Cities
NNIN REU Mentor: Jan Makowski, Electrical and Computer Engineering, University of Minnesota-Twin Cities
Contact: cyeung1@swarthmore.edu, joey@ece.umn.edu, makowski@umn.edu

Abstract/Introduction

It has been previously shown that the surface recombination velocity of exposed indium gallium arsenide (InGaAs) quantum wells can be significantly reduced by permanently placing the heterostructure in a hydroxide solution or by forming a hydroxide crystalline layer [1]. The focus of this experiment is to use temporary hydroxide treatments, which do not form a crystal layer, to improve surface quality. A step was etched into an indium phosphorus (InP)/InGaAs heterostructure to expose a quantum well. Next, half of the sample (perpendicular to the step) was covered with photoresist and the whole sample was treated with buffered oxide etch and various concentrations of sodium hydroxide (NaOH) solution. After stripping the resist, the covered side was compared to the treated side to measure the difference in photoluminescence. The measurements show that the surface treatments did not reliably improve surface quality. Specifically, with a 90% confidence level, it was determined that a 1 mM NaOH, 30 minute treatment had no effect.

The ultimate goal of this research was to improve a device being developed for nanomechanical tuning of electron states.

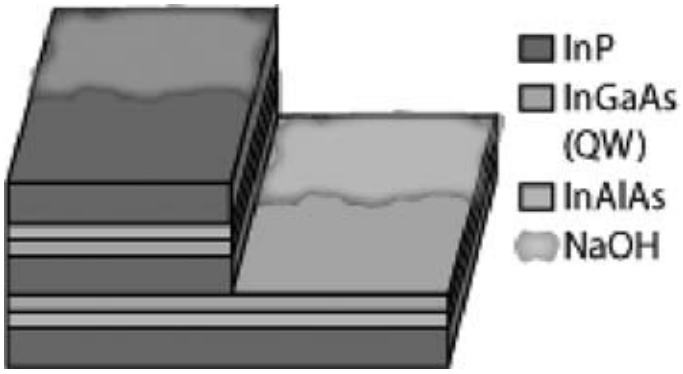

Figure 1: Four regions of the sample used in the experiment (With InP Cap/Exposed InGaAs Well, Treated or Not Treated).

Theory

InP/InGaAs Heterostructures. A quantum well is formed in a semiconductor when a thin semiconductor with a lower band gap (ex: InGaAs) is sandwiched between two thicker layers of a different semiconductor (ex: InP) with a higher band gap. Electrons within the middle layer are confined to the 2-dimensional plane of the well.

Surface Recombination. When the layer above the quantum well is etched away, the well is "exposed." The incomplete bonds at the surface create trap states. Trap states are energy levels between the conduction band and the valence band at which electron-hole pairs recombine non-radiatively. Chemical bond passivation is used to slow trapping and recombination.

Photoluminescence (PL). When photons are absorbed by a semi-conductor, electrons within the compound are excited to higher energy states. When these electrons recombine to their original state through radiative recombination, photons are emitted. The amplitude and wavelength of the emitted light can be measured to further characterize the semi-conductor which produced the PL. Because PL intensity decreases when many electron-hole pairs recombine non-radiatively at the surface, a low PL indicates a large amount of surface recombination.

Experimental Procedure

To measure the effect of the hydroxide treatment on exposed quantum wells, steps were etched into the InP/InGaAs heterostructures, exposing the quantum wells. A standard photolithography process using 1818 photoresist was used to cover half the sample with photoresist. Next, the sample was etched in a solution of HCl: H_3PO_4:CH_3COOH (1:1:2) for 120 seconds, a solution of H_2SO_4:H_2O_2:H_2O (1:8:500) for 120 seconds, and, again, a solution of HCl:H_3PO_4:CH_3COOH (1:1:2) for 90 seconds.

Because it was expected that the surface treatment only affected the exposed quantum well, the treated and untreated regions of the capped quantum well were used to check the experimental procedure. A great difference in PL of the capped regions would indicate a systemic error in the experiment.

After etching, photoresist was painted onto half of the sample (perpendicular to the step). (A standard photolithography process was not used because the developer may chemically passivate the exposed quantum well bonds.) Then, an eye-dropper was used to form a bubble of NaOH solution on the sample. After various times of treatment, the sample was rinsed with deionized (DI) water and a solvent rinse.

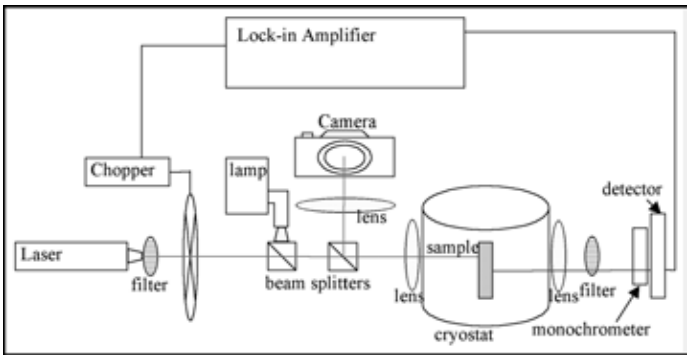

Figure 2: Apparatus for measuring photoluminescence.

The PL of four points on each of the four resulting regions was measured using the apparatus shown in Figure 2 from a frequency of 800 nm to 1750 nm, at room temperature.

Results and Conclusions

The average maximum PL of the untreated side is 1.56 pA (standard deviation = 1.26) while the average maximum PL of the treated side is 1.43 pA (standard deviation = 1.43). The means are statistically similar, with a confidence level of 90%. Treatments from 1 mM to 10 M and treatment times from 1-30 minutes were tested. A student t-test was used to analyze the data because previous experiments showed that the variation across the sample after etching, but before surface treatment, was about 100%. Therefore, only an improvement of above 100% could be attributed to the surface treatment, and not sample variation. Other experimental data indicates that the photoresist itself did not effect the PL of the samples.

Future Work

While it can be concluded that a 1 mM NaOH solution treatment for 30 minutes did not significantly improve the PL of the heterostructure, other concentrations and treatment times may have an effect. However, when the concentration was increased to 1M, the photoresist was etched away on the sample and so the control side was not preserved. A different photoresist may prevent this phenomenon.

It was also observed that longer or stronger treatments triggered a chemical reaction that resulted in a dark-colored film on the surface of the heterostructures. It would be worthwhile to experiment with other hydroxide solutions, such as potassium hydroxide (KOH), to determine if the formation of the film could be prevented. It would also be interesting to repeat this experiment, but allow a crystal layer to form, just to see if the previous results of Yablonovitch could be duplicated with this experimental apparatus.

Acknowledgments

I would like to thank Dr. Joey Talghader and Jan Makowski for their guidance. I would also like to thank Dr. Doug Ernie, the University of Minnesota ECE REU program coordinator, and the NFC staff for their efforts.

This study was funded by the National Science Foundation through the National Nanotechnology Infrastructure Network Research Experience for Undergraduates Program at the University of Minnesota, Twin Cities.

References

[1] E. Yablonovitch, H.M. Cox, T.J. Gmitter. "Nearly ideal electronic surfaces on naked InGaAs quantum wells", Appl. Phys. Lett., March 21, 1988, Volume 52, Issue 12, pp. 1002-1004.

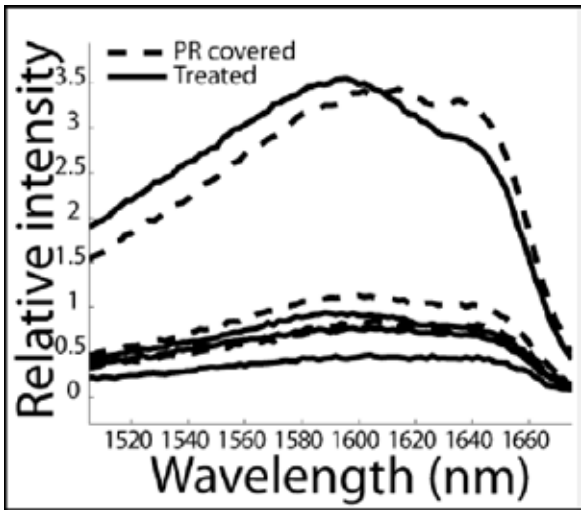

Figure 3: PL of exposed quantum well treated in 1 mM NaOH solution for 30 minutes.